Measuring the ordering of closely-packed particles

Nizan Meitav and Erez N. Ribak[a)]
Department of Physics, Technion – Israel Institute of Technology, Haifa 32000, Israel

We look at irregularity and phase transitions in two-dimensional patterns. Two independent methods are provided for identifying and measuring hexagonal close packing of particles. We implemented these methods on images of melting colloidal films at different melting processes. We could easily spot various defects in the hexagonal crystal film. The feasibility of the methods is also demonstrated on human retinal images, for measuring the unit cell size and fraction of close-packed cone photoreceptors.

Statistical analysis indicates that phase transition in two-dimensions (2D) is quite different from three dimensions. For instance the XY model predicts algebraic dependence of the correlation function at low temperatures preceding the exponentially decaying one. There are various theories of the mechanism of melting of 2D layers: formation of grains boundaries[1], formation of topological defects prior to the transition[2], etc. One of the main theories of phase transition by lattice defects predicts a continuous phase transition into an intermediate phase form, the hexatic phase, by dislocations of pairs in the lattice[2,3]. Unbinding these pairs reduces the translational order into short range, and orientation order into quasi-long range. Consequently, it is important to identify changes in the shapes of lattices not only for detection of local defects but also for other forms of transitions.

The 2D arrangement of retinal photoreceptors plays a major role in determining the visual resolution (the eye size is much larger than the receptor spacing). Better acuity can be achieved with higher photoreceptors density, the maximum obtained by hexagonal closed packing.[4] Our brain is unable to handle that many inputs, so only ~1mm^2 of the retina has contiguous closely packed cones, and their density decreases rapidly towards the periphery. These are studied by high resolution imaging down to single photoreceptors, first cones[5,6] and then even smaller rods.[7,8] We are interested in the grid of cones in order to understand how the eye samples an image.

We introduce two analysis methods of hexagonal patterns of particles. The first method is based on angular analysis of the image's Fourier transform to measure the size of the hexagons, and it functions even when the number of hexagons is low, and their symmetry is hardly detectable. The second method employs a matched filter to identify the hexagonal pattern.

The mean hexagon size measurement makes use of the six-vertex symmetry of the Fourier spectrum of triangles. As hexagons come in different and varying orientations, their transform is smeared into a circle[9], and the analysis has to be performed piecewise (Fig. 1). First the image was sectioned into patches corresponding to the short range order, such that most hexagons were more or less oriented in the same direction. The power spectrum of each section was converted from Cartesian into polar coordinates, $(u, v) \rightarrow (\rho, \theta)$, in order to identify the six-vertex symmetry. In polar coordinates hexagons should show as six maxima at a constant period along the angle axis, if indeed derived from a mosaic of uniformly arranged triangles in the spatial domain. The six points may not be distinct enough in the (ρ, θ) plane due to the different hexagon orientations and local density variation. To improve visibility, the angular content of the power spectrum was Fourier transformed in one dimension (1D),

$$F(\rho,\omega) = \int \left| f(\rho,\theta) \right|^2 \exp(-2\pi i\theta\omega)\, d\theta \qquad (1)$$

where $f(\rho, \theta)$ is the 2D Fourier transform of the image expressed in polar coordinates, and $F(\rho, \omega)$ is the image power spectrum in terms of radius and angular frequency. $F(\rho, 6)$, represents a frequency consisting of six equidistant vertices, regardless of the orientation of the hexagonal packing (similar to q_6 in Ref. 2). The average size of the hexagons is the

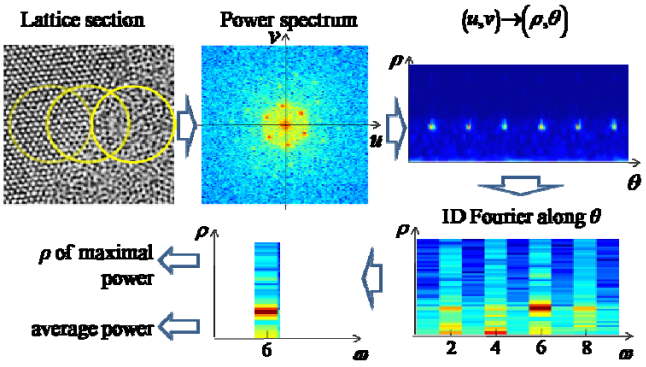

Fig. 1 (color online). Sizing the hexagons. Section by section of the lattice is Fourier transformed and converted to polar coordinates. Then only the angular direction is 1D Fourier transformed. The signal at the sixth frequency is analyzed for the location of the maximum and its value (shown for the rightmost section).

value of ρ where the maximal power of $F(\rho, 6)$ occurs; its phase is the orientation angle, ignored here. Results were averaged over all sections to obtain the mean $F(\rho, 6)$. To increase sampling, sections overlapped by half their size. The efficacy of this method was tested on an artificial grid of hexagons, each of size of 2.69 pixels. The hexagon side was found to be 2.67 pixels, less than 1% disagreement.

In the second method, we identified the hexagons positions in the lattice by applying a hexagonal matched filter on the image. The matched filter size was determined by the mean hexagon size calculated in the above method. For retinal images we used two different sizes of masks, as photoreceptors size varies across the retina. To account for different hexagon orientations, it was sufficient to rotate each mask also by two more steps of $\pi/9$. Each of the filtered (or cross correlated) images was diluted by leaving only its local maxima. Then a threshold was applied to the histogram of the maxima to remove the filter-noise correlations. For ordered arrays, each of the hexagon correlation maxima was surrounded by lower near-neighbor correlations[9]. Thus the threshold was tuned by requiring only one correlation maximum for each hexagon in these images (ordered parts of Fig. 2). The final result was converted to a binary image.

In order to diminish the effect of different light levels at different areas, we employed a normalized cross correlation[10]

$$\gamma(\mathbf{w}) = \frac{\sum_{\mathbf{x}}[f(\mathbf{x}) - \overline{f}_{\mathbf{w}}][t(\mathbf{x}-\mathbf{w}) - \overline{t}]}{\left\{\sum_{\mathbf{x}}[f(\mathbf{x}) - \overline{f}_{\mathbf{w}}]^2 \sum_{\mathbf{x}}[t(\mathbf{x}-\mathbf{w}) - \overline{t}]^2\right\}^{0.5}} \quad (2)$$

where t is the template mask (i. e. a mask of hexagon vertices), $f(\mathbf{x})$ is the image, $\overline{f}_{\mathbf{w}}$ is the mean of $f(\mathbf{x})$ in the region under the template and $\overline{t}$ is the mean of the template.

Another quantity calculated was the fraction of hexagons out of cells or particles. For that we repeated the same analysis, but instead of taking a hexagonal mask we used a circular one to locate single cells. The two binary images (hexagons and cells) were first smoothed into continuous ones, then divided to yield the local fraction of hexagons.

For retinal analysis the threshold was calibrated by requiring that density of single cells agreed with the ex-vivo data for the same retinal region[11]. When the threshold value was changed simultaneously for both steps of the analysis (hexagons and later cells) it had little influence on the ratio.

To test the reliability of this method we applied it to artificial images made of one hexagon, placed among randomly positioned particles, which occurs in both colloids and retinal tissue. We could identify the hexagon out of 1000 such particles. For the phase transition analysis we used images of different melting processes of a colloidal film of varying thickness[12]. For thick, 12 layer films (Fig. 2 a,b,c) the grain boundary melting forms a wide strip and indeed the hexagonal lattice is reduced to floating individuals. In a thin, 4 layers film (Fig. 2 g,h,i), the hexagon map is made of local

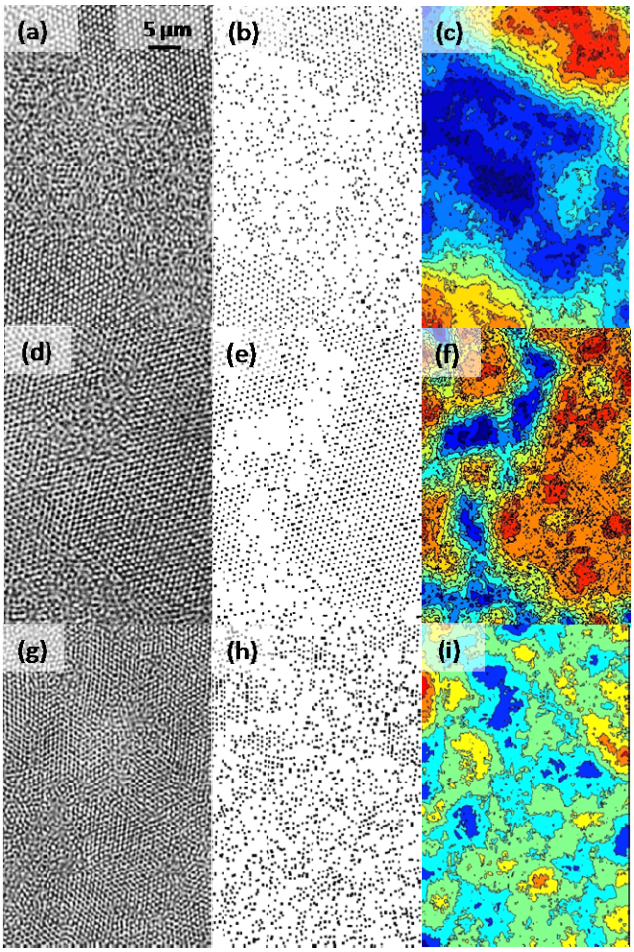

Fig 2. (color online). Left column: Melting processes for 12, 5, and 4 layer thickness, imaged at different magnifications and occasional blurring. Center: Corresponding hexagons' positions, after using the matched filter and thershold. Right: Positions smoothed by a circular filter into hexagons' density contours, hot color signifying high density. Images courtesy of Y. Peng, Physics Dept., Hong Kong University of Science and Technology.

clusters of defects all over the lattice. For an intermediate 5 layers thickness, melting was spotted both at the liquid strip and the "lake", inside the domain, by lack of hexagon arrangement in those areas (Fig 2 d,e,f). It seems that lattice order was also starting to break in the area between the "lake" and the strip, maybe indicating on a start of a merging process. The size of the smoothing filter in the right column was varied with the size of the melting area. For the 12 layers thickness, which has a big molten strip, we used a bigger smoothing filter, ~10×cell size, so that the perimeter of the solid could be identified with a specific contour. For 4 and 5 layers, where the effect is more local, we used ~7×cells size filter.

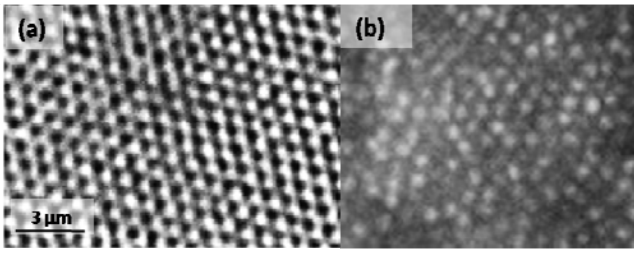

Fig 3. (a) A defect detected in hexagonal lattice of colloidal particles (Fig. 2a). (b) Photoreceptors mosaic (~7µm spacing), courtesy of Dr. Laurent Vabre, Imagine Eyes Ltd., France.

The mean hexagon size method yielded sizes of 5.7, 7.6 and 9.0 pixels for 4, 5, and 12 layers, to be compared with manually averaged values of 6.0, 7.8 and 9.2 pixels. The average power of $F(\rho, 6)$ was three order of magnitude higher than $F(\rho, 5)$ and $F(\rho, 7)$, indicating the dominance of hexagonal patterns. Fig. 3a is a magnified right part of Fig. 2d, exactly where Fig. 2e indicates a defect in the lattice.

For retinal analysis we used off-center locations (nasal parafovea) measured by others and by us[4,5]. Fig. 3b is a region of the retina showing the cones. First we assumed that some of these cells are arranged in hexagonal packing, and estimated manually the nearest neighbors spacing to be 10.8 pixels. Then we implemented our hexagon size method on this image, and the result was 11.1 pixels.

In order to check the percentage of hexagonal packed cells, we used a retinal image that was measured using Voronoi diagram[4] (their Fig. 3d). The fraction of hexagons was 60% compared to their 57%. Fig. 4 displays locations of cells and hexagons in a retinal image, including part of the optic disc at the bottom right. We used our images and improved their resolution by weighted shift-and-add sub-pixel registration[5]. As expected, in the optic disc the number of cones, hexagons and their ratio (Fig. 4 b,c,d) is much lower than in the other parts of the image. The fraction of hexagons (Fig. 4d) inside the disc is less than 10% (it should be zero), providing the level of error. Artifacts inside the large blood vessels (Fig 4b) caused this deviation. In other parts of this image the hexagon fraction was up to 30%. By implementing the mean hexagonal size method on Fig. 4a (excluding the optic disc), we found that the mean size is 7.69 µm. This agrees with the minimum spacing between cones, which is roughly constant at 6-8 µm across most of the retina.[13]

In summary, two independent methods were presented for detecting and measuring the size of hexagonally packed particles. By being sensitive even to a small deviation in the pattern of particles, these methods enable early detection and characterization of phase transitions. By using the same technique for measuring single cells in the retina, the local fraction of close-packed photoreceptors was quantified. The distinction of these non-morphological methods is the ability to measure the hexagonal properties where pattern discontinuity occurs, for instance melting boundaries, or the arrangement of cells near blood vessels. Notice that the matched filter method can be used for detecting other repetitive patterns by corresponding masks, for example in small grains, where the eye is the final judge today.

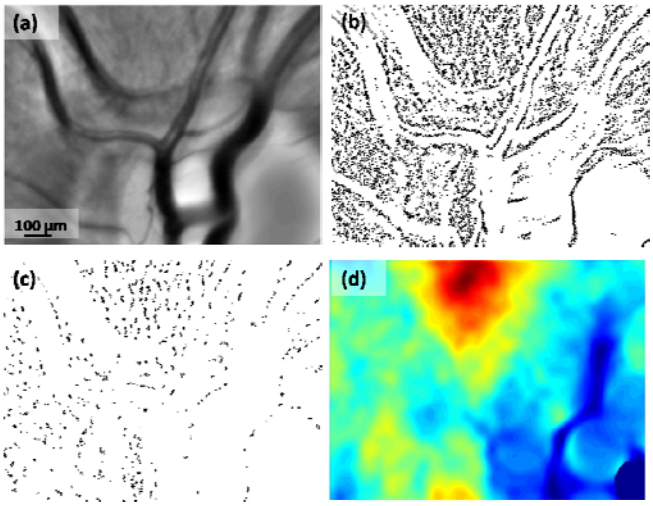

Fig 4. (color online). (a) Retinal image[5] of the optic disc and its vicinity (size 1.4×1 mm^2). (b) Cells positions using a round matched filter. (c) Hexagons position using hexagonal filter. (d) The fraction of hexagons out of single cells varies from 30% to 0% (hot to cold color).

This work was supported in parts of by the Israel Science Foundation and by the Walton Fellowship of Science Foundation Ireland.

[1] S.T Chui, Phys. Rev. Lett. **48,** 933 (1982).
[2] J. M. Kosterlitz and D. J. Thouless, J. Phys. C **6**, 1181 (1972).
[3] U. Gasser, C. Eisenmann, G. Maret, and P. Keim, Chem. Phys. Chem. **11,** 963 (2010).
[4] K. Y. Li and A. Roorda, J. Opt. Soc. Am. A. **24**, 1358 (2007).
[5] N. Meitav and E.N. Ribak, J. Opt. Soc. Am. A. **28**, 1395 (2011).
[6] J. Liang, D. R. Williams, J. Opt. Soc. Am. A. **14**, 2884 (1997).
[7] N. Doble, S. S. Choi, J. L. Codona, J. Christou, J. M. Enoch, and D. R. Williams, Opt. Lett, **36,** 31 (2011)
[8] A. Dubra, Y. Sulai, J. L. Norris, R. F. Cooper, A. M. Dubis, D. R. Williams and J. Carroll, Biomed. Opt. Express, **2,** 1864 (2011).
[9] A. V. Petukhov, D. van der Beek, R. P. A. Dullens, I. P. Dolbnya, G. J. Vroege, and H. N. W. Lekkerkerker, Phys. Rev. Lett. **95**, 077801 (2005)
[10] R.C. Gonzalez and R.E. Woods, *Digital image processing*. Prentice Hall (2007).
[11] C. A. Curcio, K. R. Sloan, R. E. Kalina and A. E. Hendrickson, J. Comp. Neurol. **292**, 497 (1990).
[12] P. Y. Peng, Z. Wang, A.M. Alsayed, A.G. Yodh and Y. Han, Phys. Rev. Lett. **104**, 205703 (2010).
[13] C. A. Curcio and K. R. Sloan, Vis. Neuroscience, **9**, 169 (1992).